Appendix D

Supplementary Information for Chapter 5: Argentination: a silver bullet for cannabinoid analysis by DMS-MS^2

This appendix contains the supporting information for Chapter 5, and is analogous to the supporting information to the following manuscript:

Ieritano, C., Thomas, P., Hopkins, W. S. Argentination: A Silver Bullet for Cannabinoid Analysis by Differential Mobility Spectrometry. *Anal. Chem.* **2023**. 95 (22), 8668 – 8678.

https://pubs.acs.org/doi/abs/10.1021/acs.analchem.3c01241

Table of Contents

Supporting Figures and Tables 3

Supplementary Sections 26

S5-1 – Computational Methods 26

Section S5-2. Computational investigation of the fragmentation behaviour of argentinated Δ^8-THC, Δ^9-THC, CBD, and CBC. 29

Section S5-3. Computational investigation of the fragmentation behaviour of argentinated exo-THC, CBN, and CBG 32

Section 5-4. Frequently Asked Questions 33

References 34

Supporting Figures and Tables

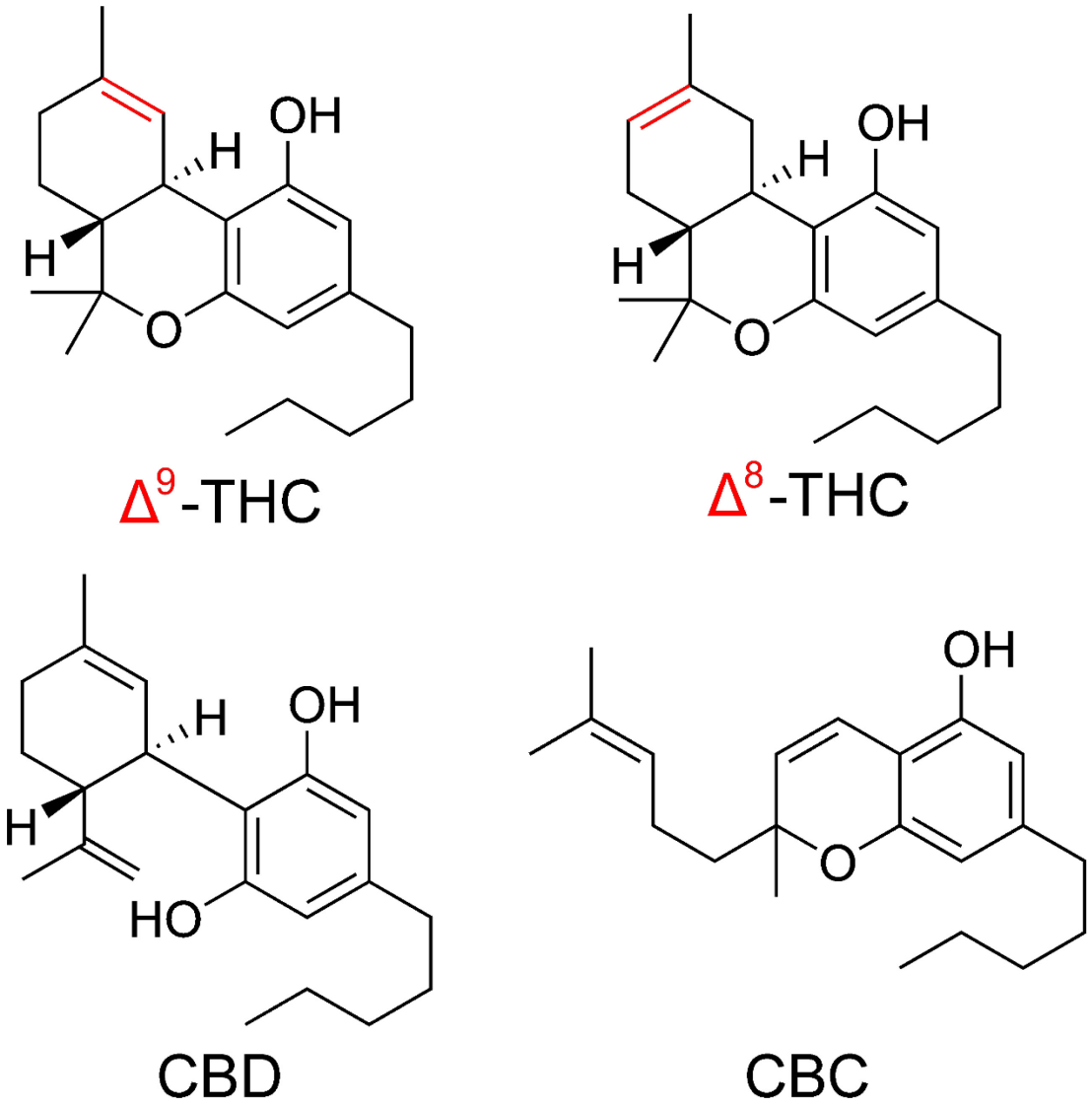

Figure S5-1. Structures of Δ^9-THC, Δ^8-THC, CBD, and CBC. Differences in double bond position between Δ^8/Δ^9-THC are highlighted in red.

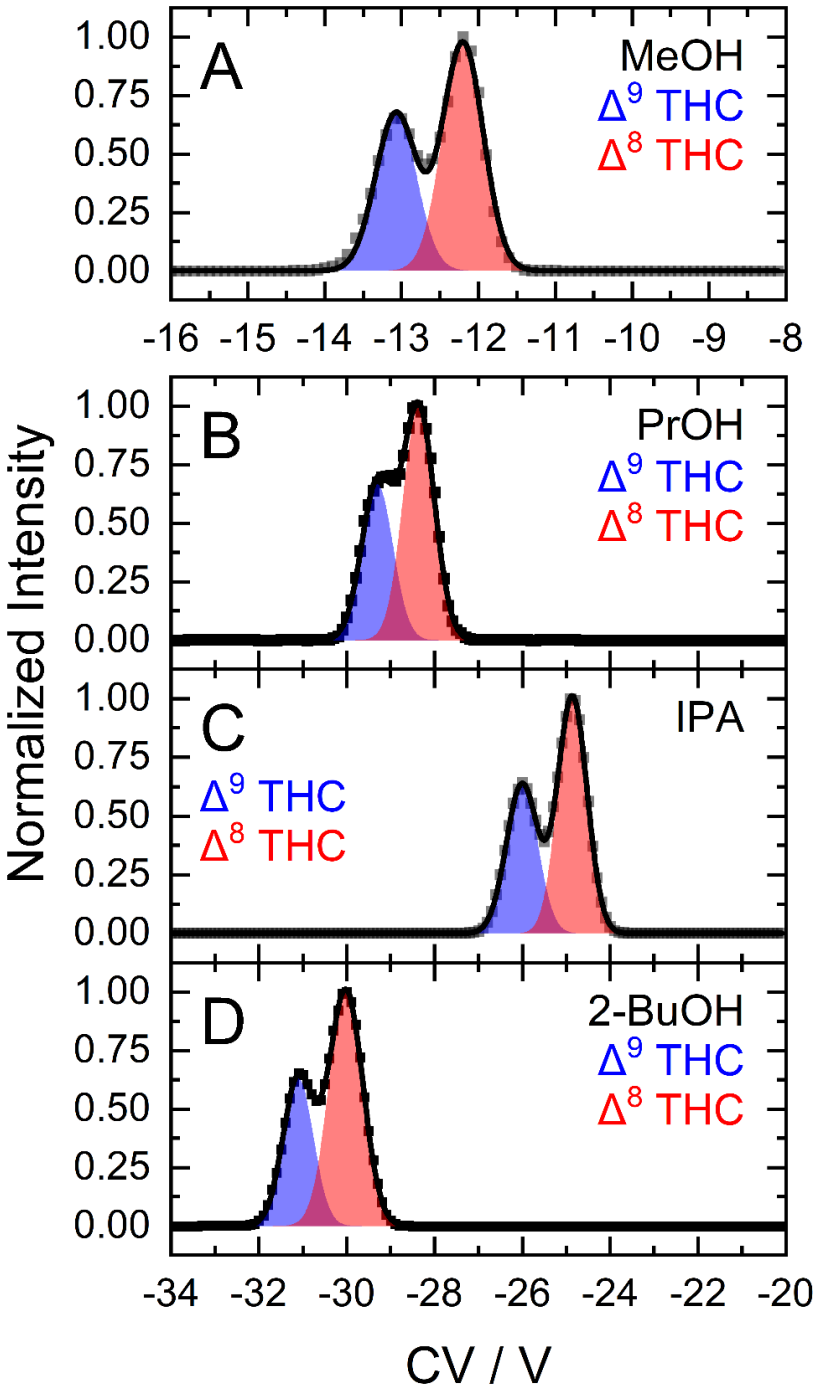

Figure S5-2. Ionograms of a 1:1 mixture of Δ^9-THC and Δ^8-THC. Analytes were monitored as deprotonated ions ($[M - H]^-$; *m/z* 313) in an N_2 DMS environment seeded with 1.5 mol% of (**A**) MeOH, (**B**) 1-propanol, (**C**) IPA, and (**D**) 2-butanol at SV = 4500 V and DT = 150 °C. 25 psi of resolving gas (DR gas; N_2) was introduced to improve resolving power.

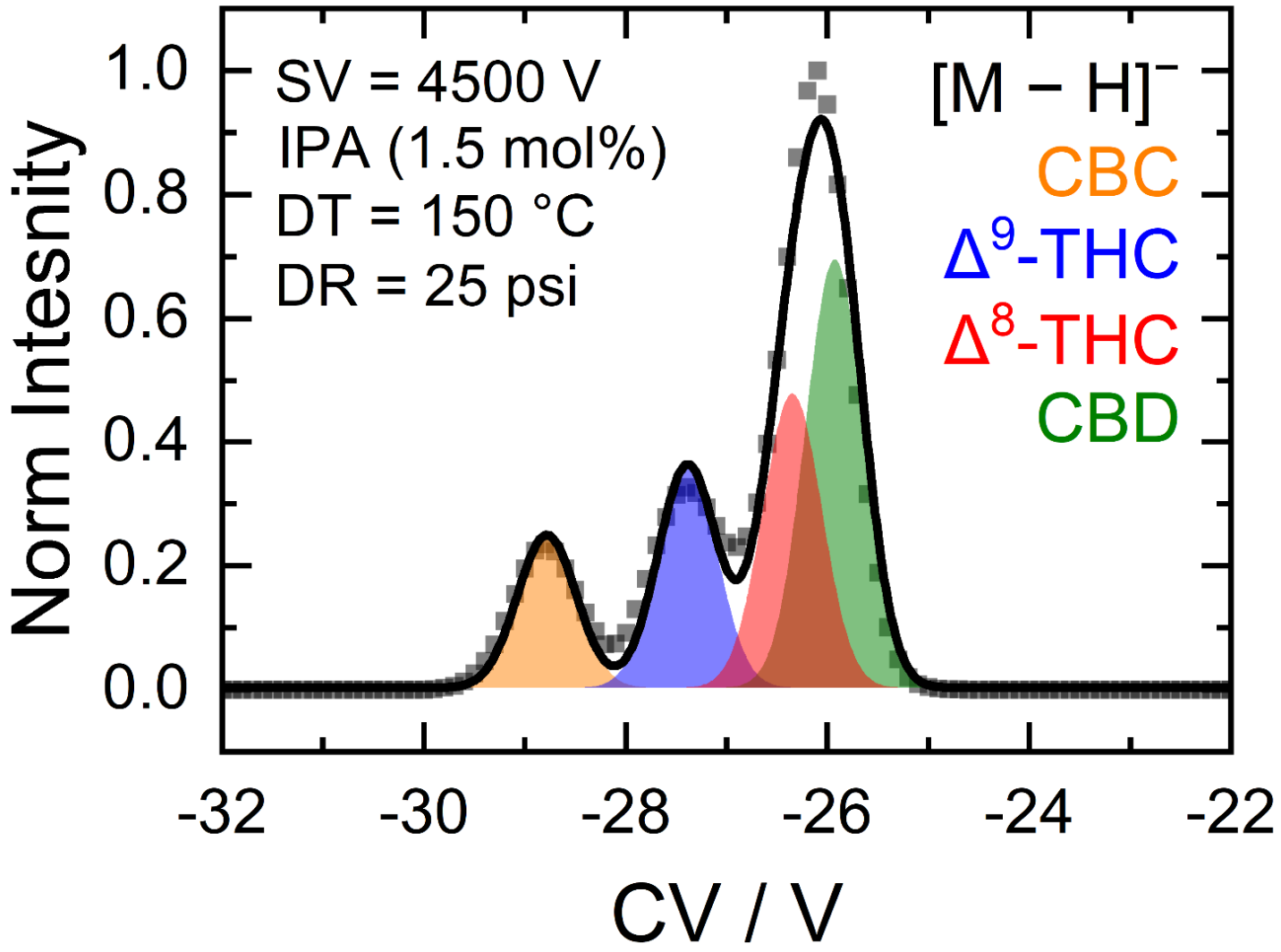

Figure S5-3. Ionograms of a 1:1:1:1 mixture of CBC, Δ^9-THC, Δ^8-THC, and CBC. Analytes were monitored as deprotonated ions ($[M - H]^-$; *m/z* 313) in an N_2 DMS environment seeded with 1.5 mol% of IPA at SV = 4500 V and DT = 150 °C. 25 psi of resolving gas (DR gas; N_2) was introduced to improve resolving power.

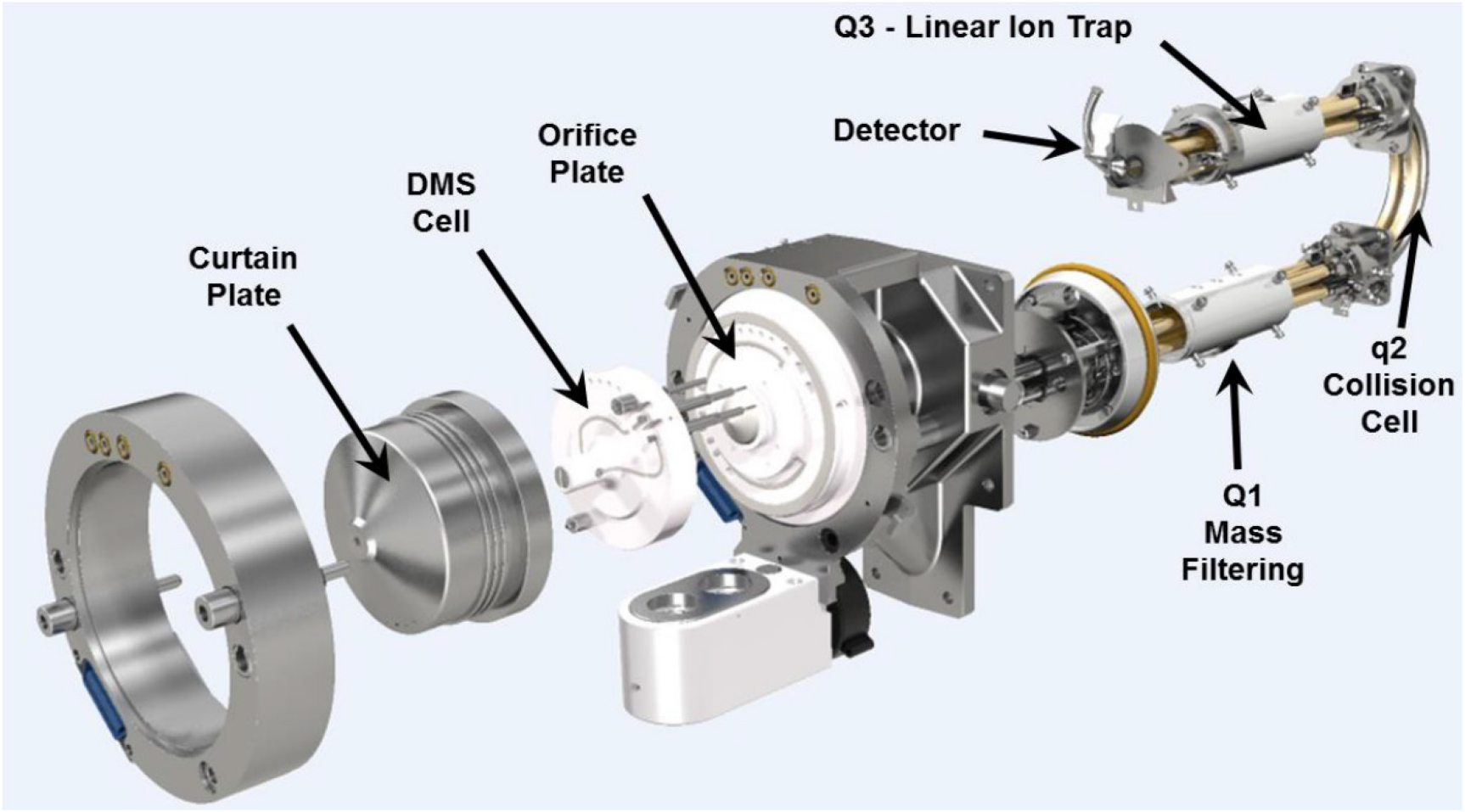

Figure S5-4. Schematic of the SELEXION system coupled to the QTRAP 5500 (SCIEX) hybrid linear ion trap triple-quadrupole mass spectrometer.

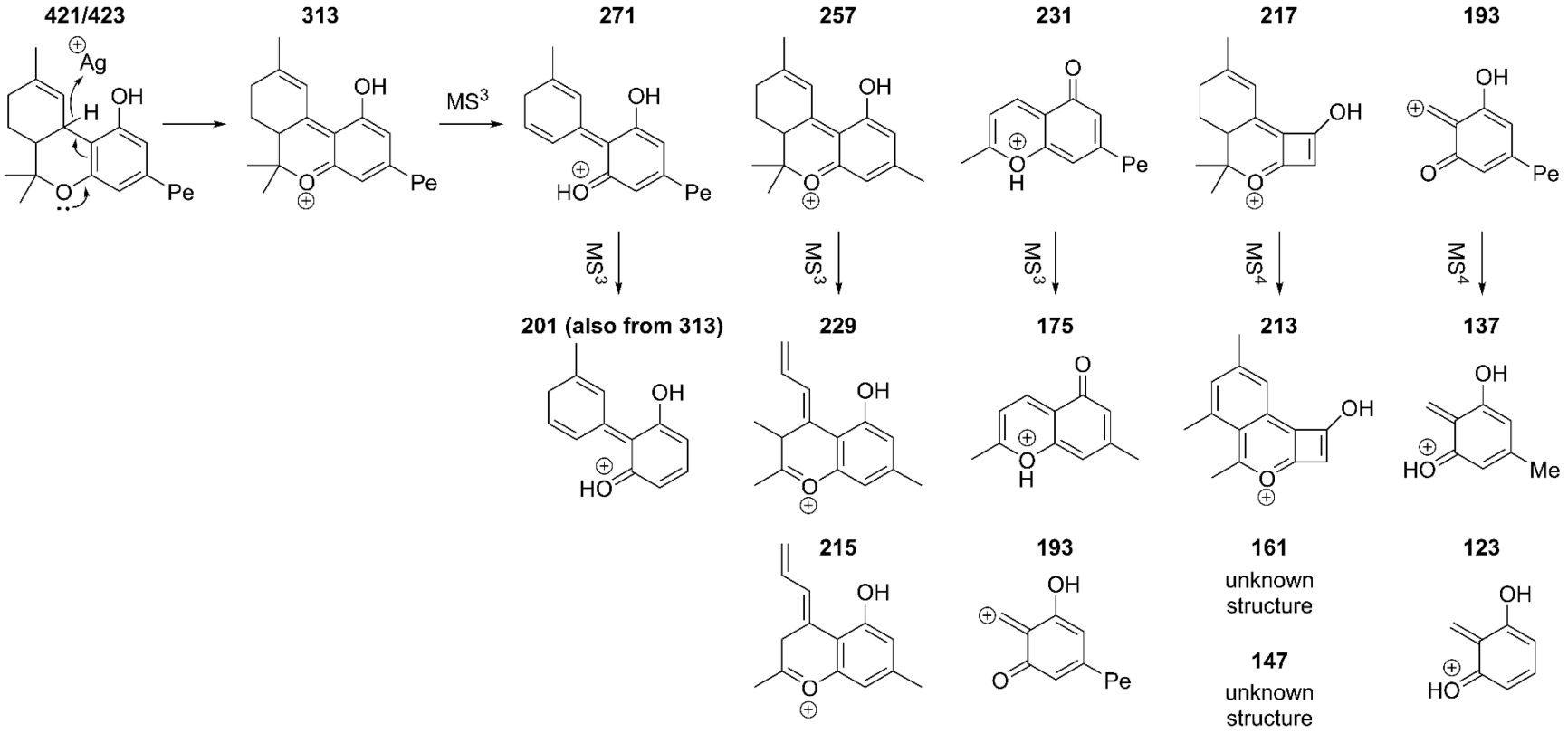

Figure S5-5. Proposed fragmentation pathway for $[\Delta^9\text{-THC} + \text{Ag}]^+$.

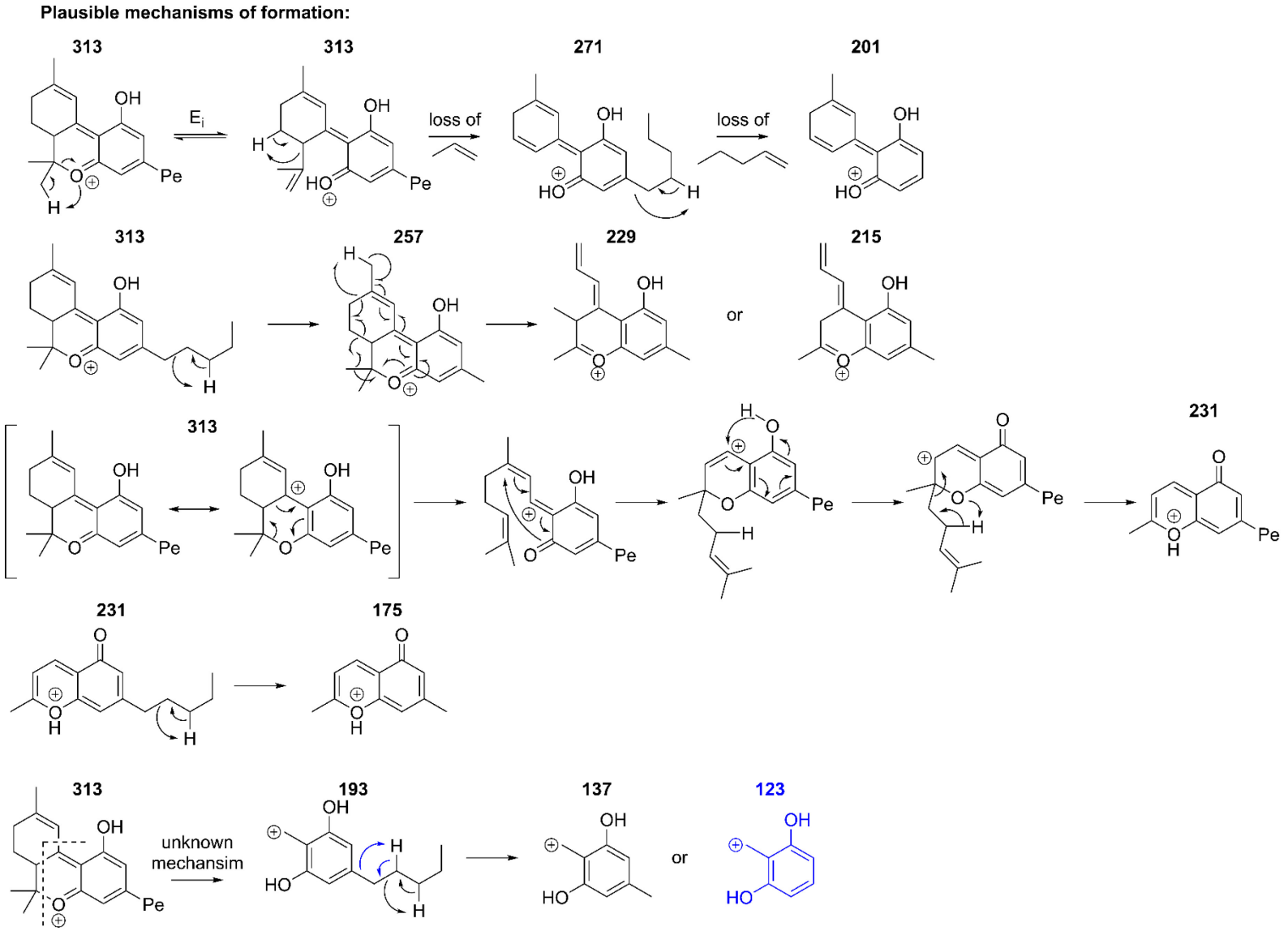

Figure S5-6. Proposed mechanisms of formation for fragments originating from $[\Delta^9\text{-THC} + \text{Ag}]^+$.

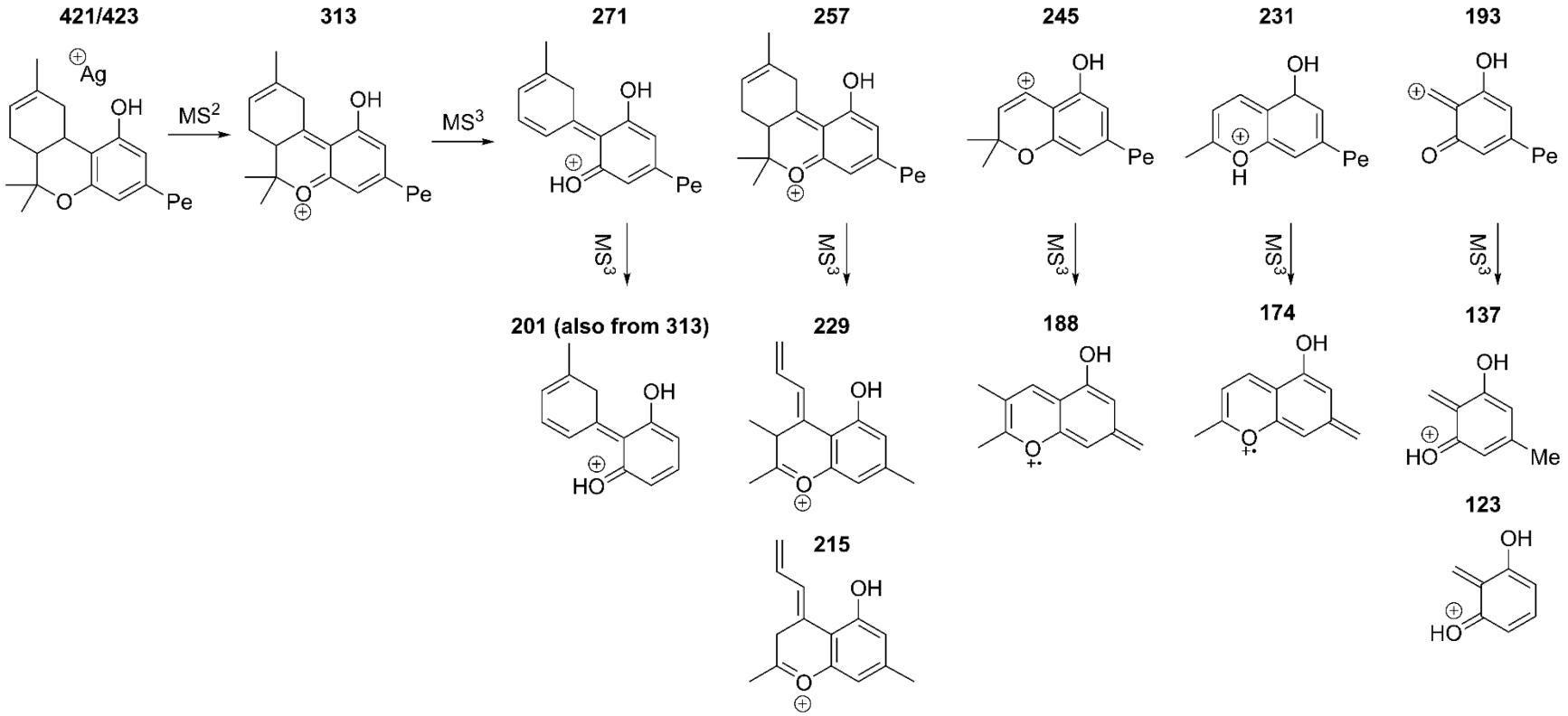

Figure S5-7. Proposed fragmentation pathway for $[\Delta^8\text{-THC} + \text{Ag}]^+$.

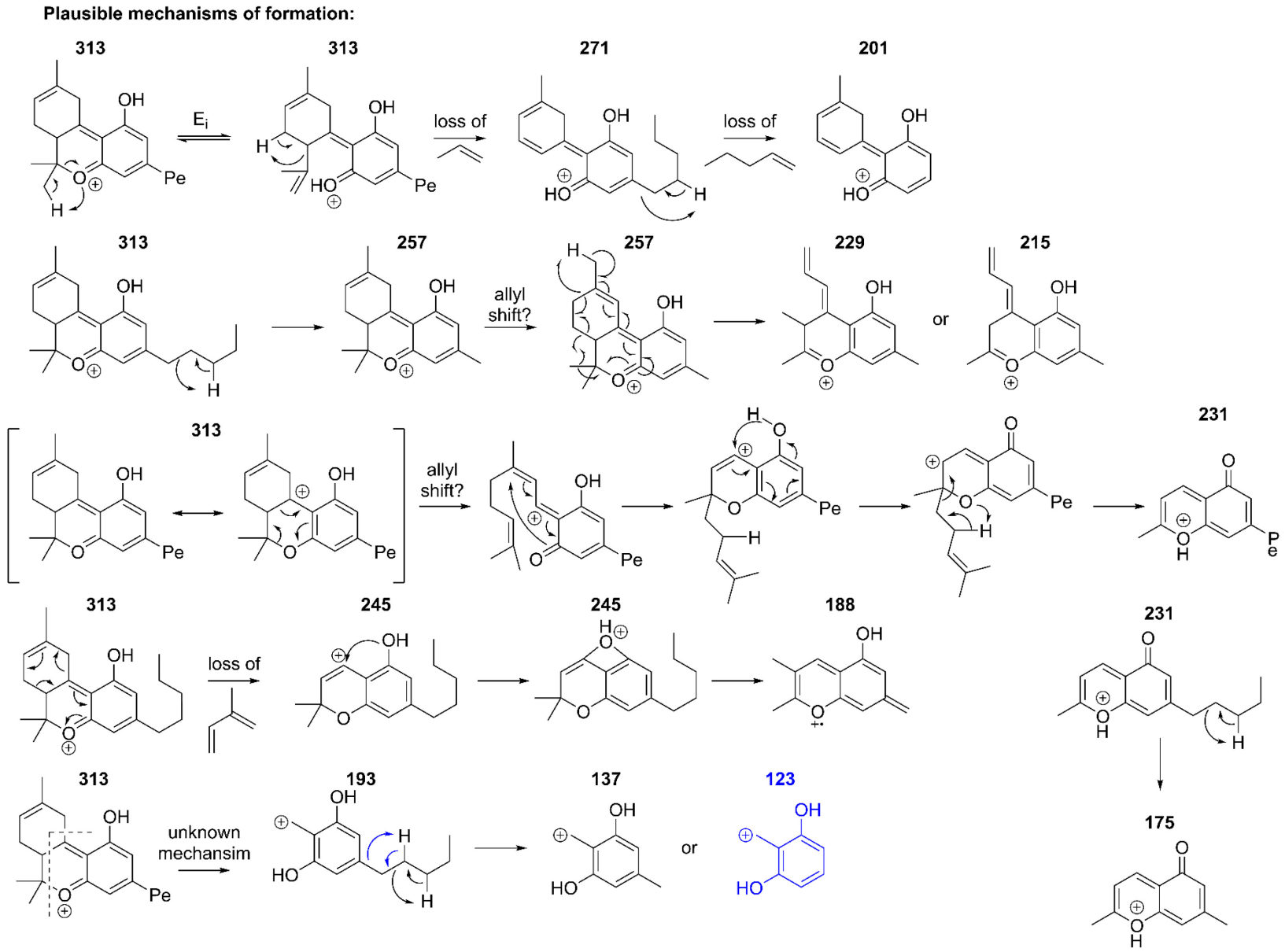

Figure S5-8. Proposed mechanisms of formation for fragments originating from $[\Delta^8\text{-THC} + \text{Ag}]^+$.

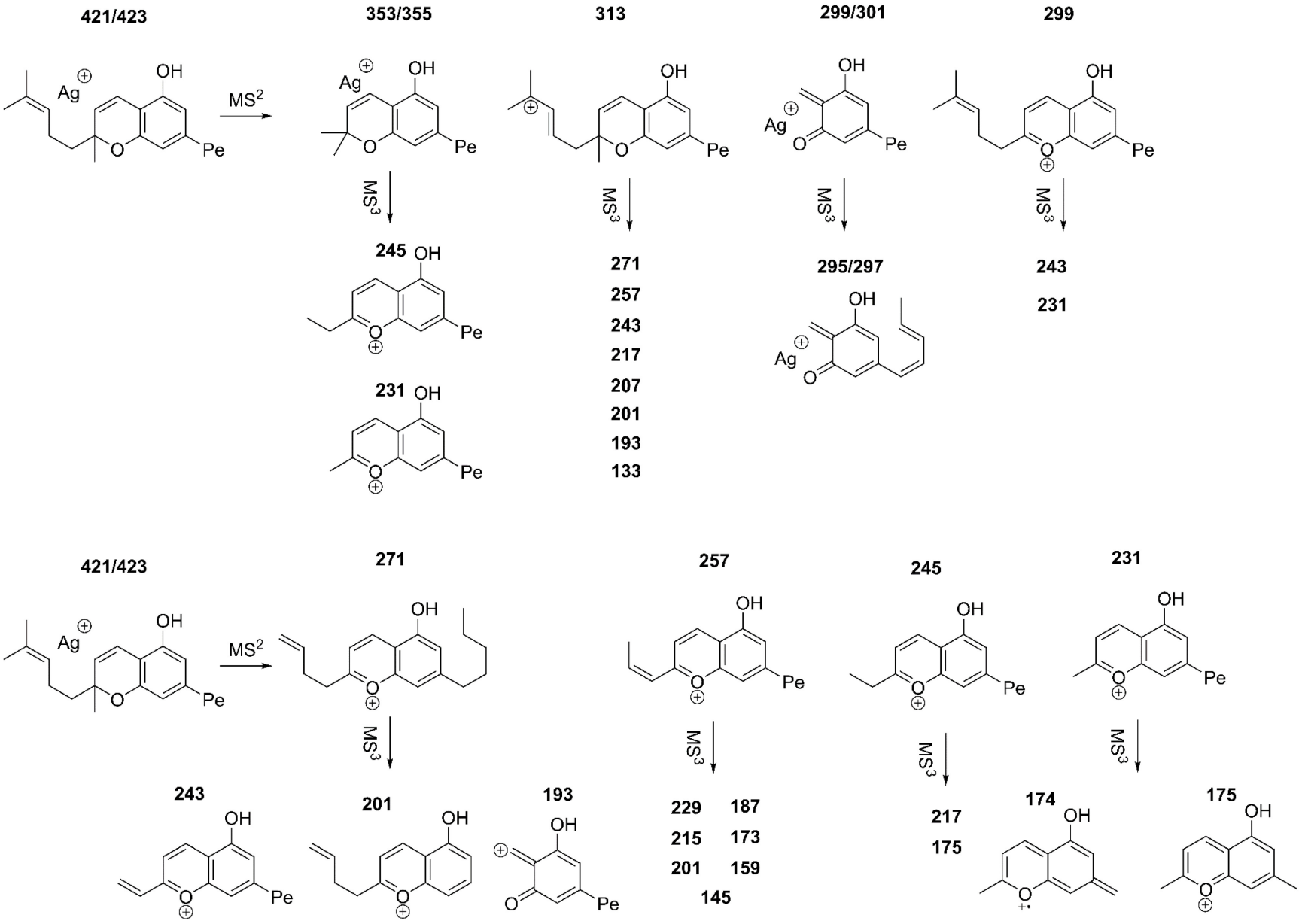

Figure S5-9. Proposed fragmentation pathway for [CBC + Ag]$^+$.

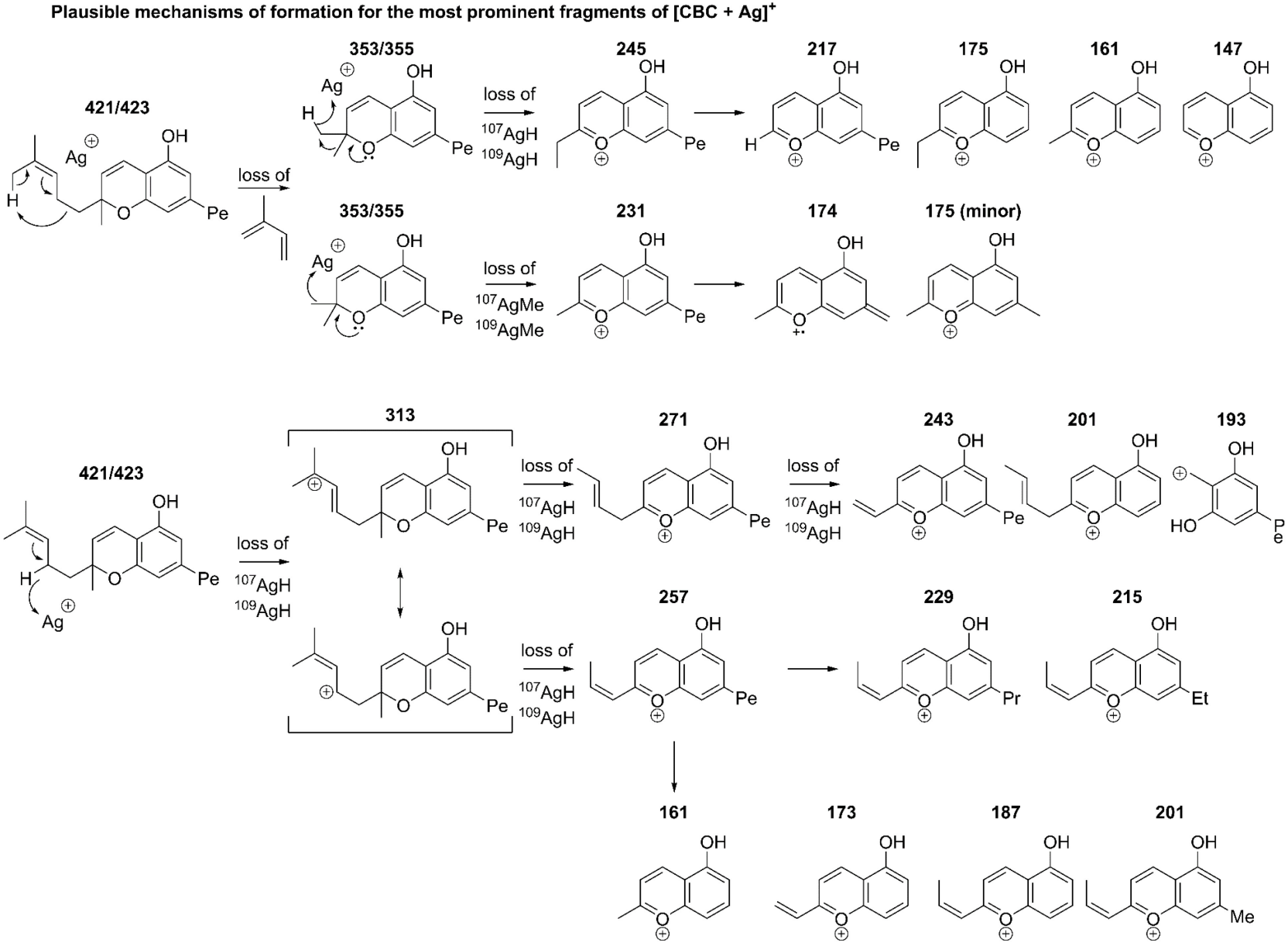

Figure S5-10. Proposed mechanisms of formation for fragments originating from [CBC + Ag]$^+$.

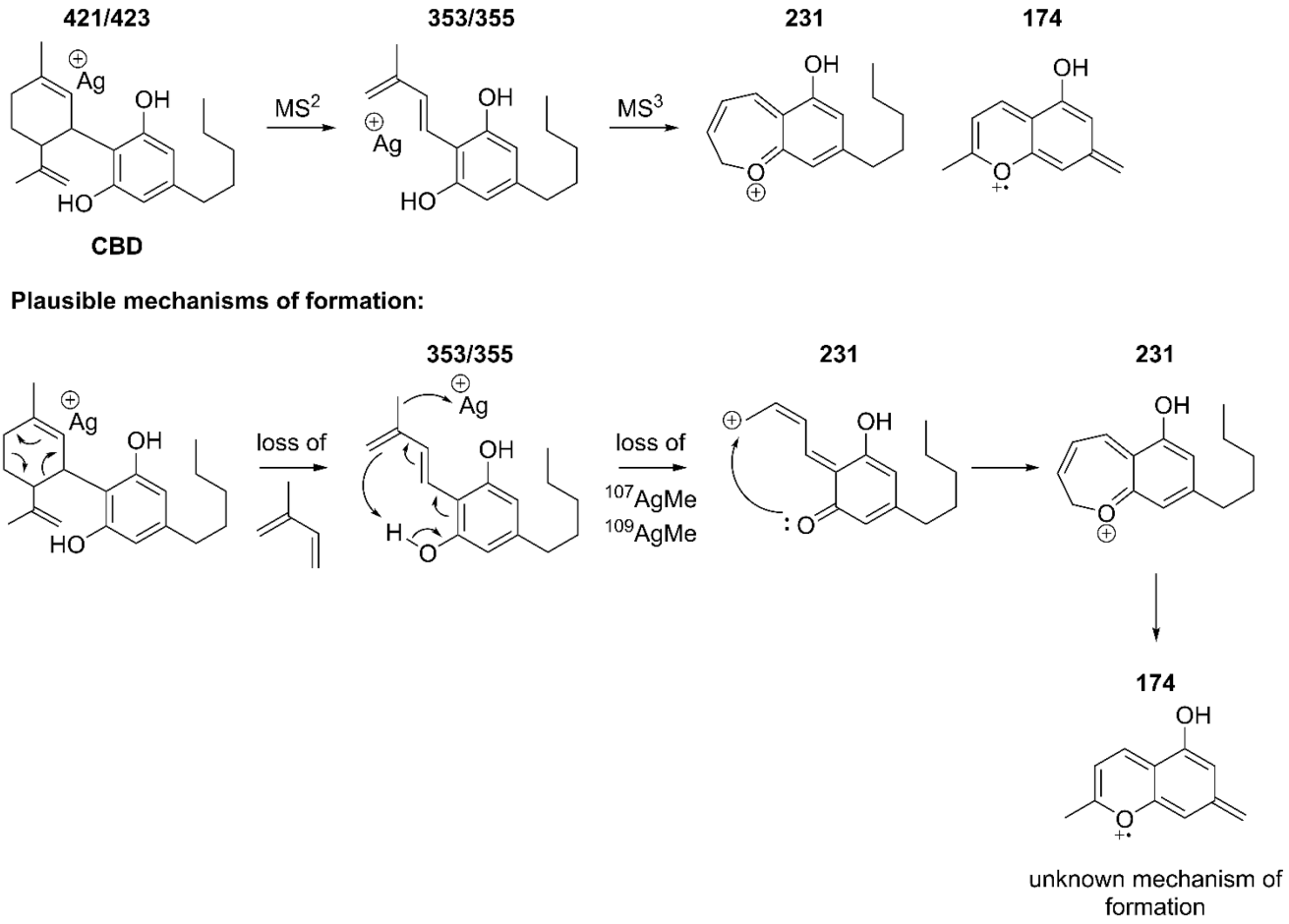

Figure S5-11. Proposed fragmentation pathway and mechanisms of formation for fragments originating from [CBD + Ag]$^+$.

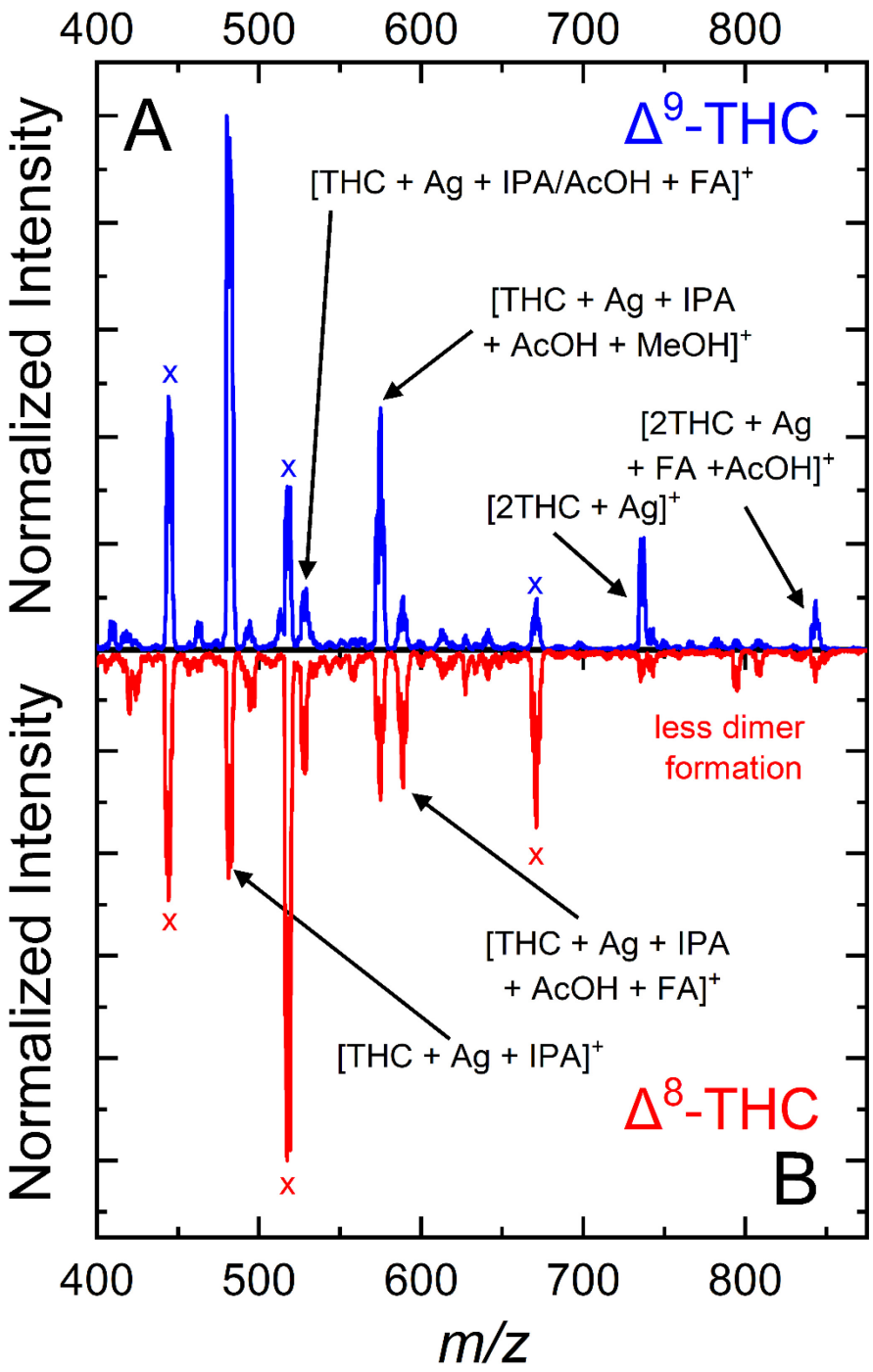

Figure S5-12. Q1 full scan mass spectrum of (**A**) $[\Delta^9\text{-THC} + \text{Ag}]^+$ and (**B**) $[\Delta^8\text{-THC} + \text{Ag}]^+$ produced via ESI from H_2O/MeOH (50:50 w/ 0.1% HCOOH) containing 1 ppm of Δ^8-THC/Δ^9-THC and 5 ppm of AgOAc. 1.5 mol% of IPA was seeded into the carrier gas (N_2), causing formation of ion-solvent clusters. Note that AcOH = acetic acid, IPA = isopropyl alcohol, FA = formic acid, and *x* denotes a species that does not contain Δ^8-THC/Δ^9-THC.

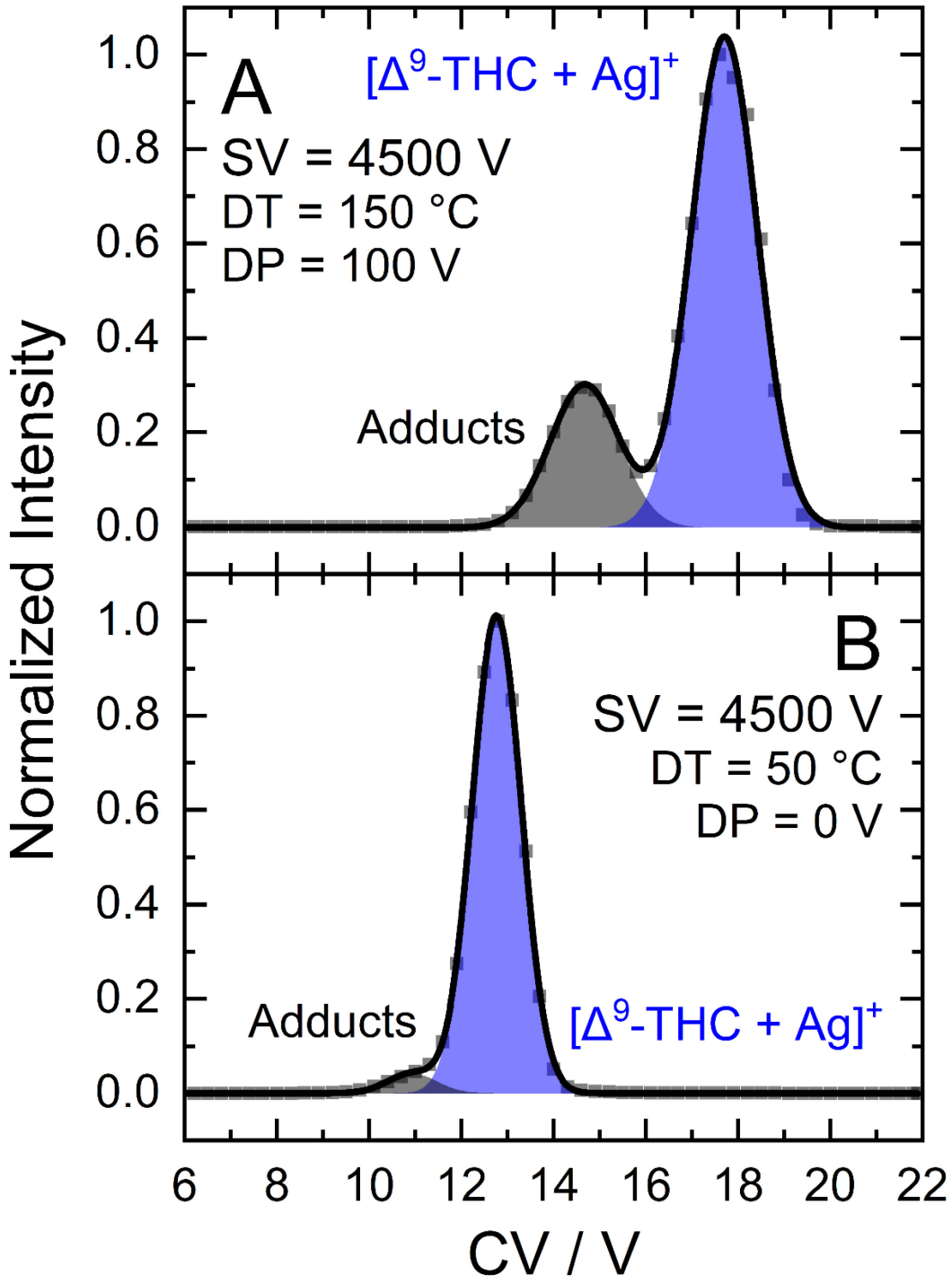

Figure S5-13. Ionogram of $[\Delta^9\text{-THC} + \text{Ag}]^+$ obtained at (**A**) SV = 4500 V, DT = 150 °C, and DP = 100 V, or (**B**) SV = 4500 V, DT = 50 °C, and DP = 0 V. Reducing DT and DP mitigates the dissociation of the $[\Delta^9\text{-THC} + \text{Ag} + \text{AcOH}]^+$ and $[\Delta^9\text{-THC} + \text{Ag} + \text{AcOH} + \text{MeOH}]^+$ adducts that give rise to the additional peak in panel A.

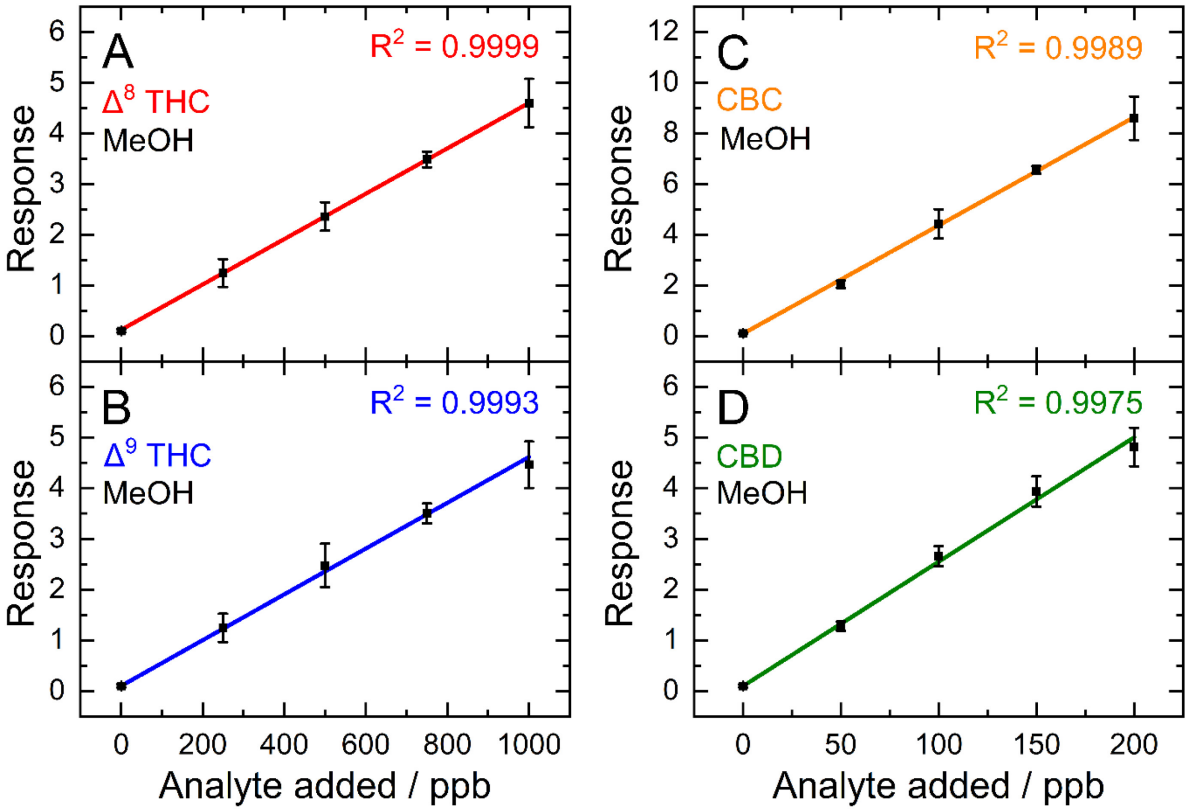

Figure S5-14. Calibration curves from concurrent standard additions of (**A**) Δ^8-THC, (**B**) Δ^9-THC, (**C**) CBC, and (**D**) CBD to a solution of MeOH containing 5 ppm of AgOAc. Error bars correspond to the standard deviation of the analyte response relative to the internal standard (CBDA; 200 ppb) across three replicate measurements.

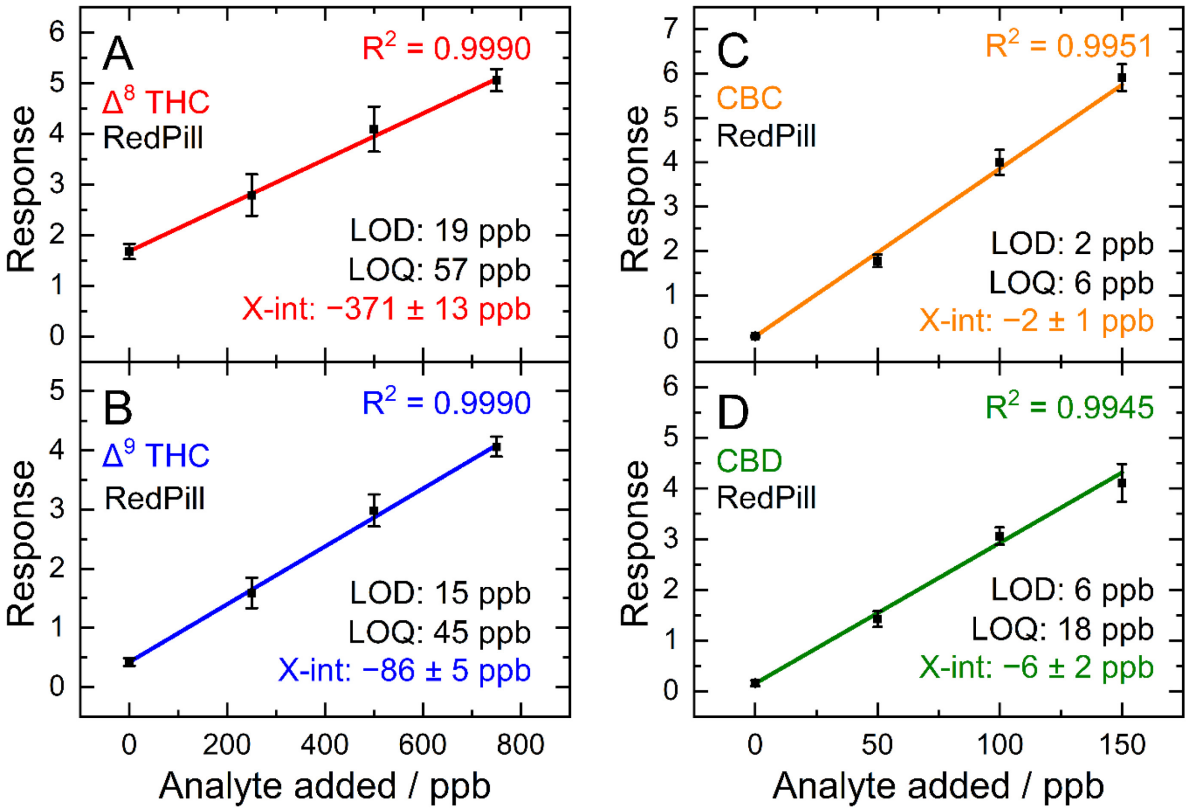

Figure S5-15. Calibration curves from concurrent standard additions of (**A**) Δ^8-THC, (**B**) Δ^9-THC, (**C**) CBC, and (**D**) CBD to the RedPill extract (50000-fold dilution in MeOH and doped with 5 ppm of AgOAc). Error bars correspond to the standard deviation of the analyte response relative to the internal standard (CBDA; 200 ppb) across three replicate measurements. Limits of detection (LOD) and limits of quantitation (LOQ) are using Equations 4 and 5 (see main text).

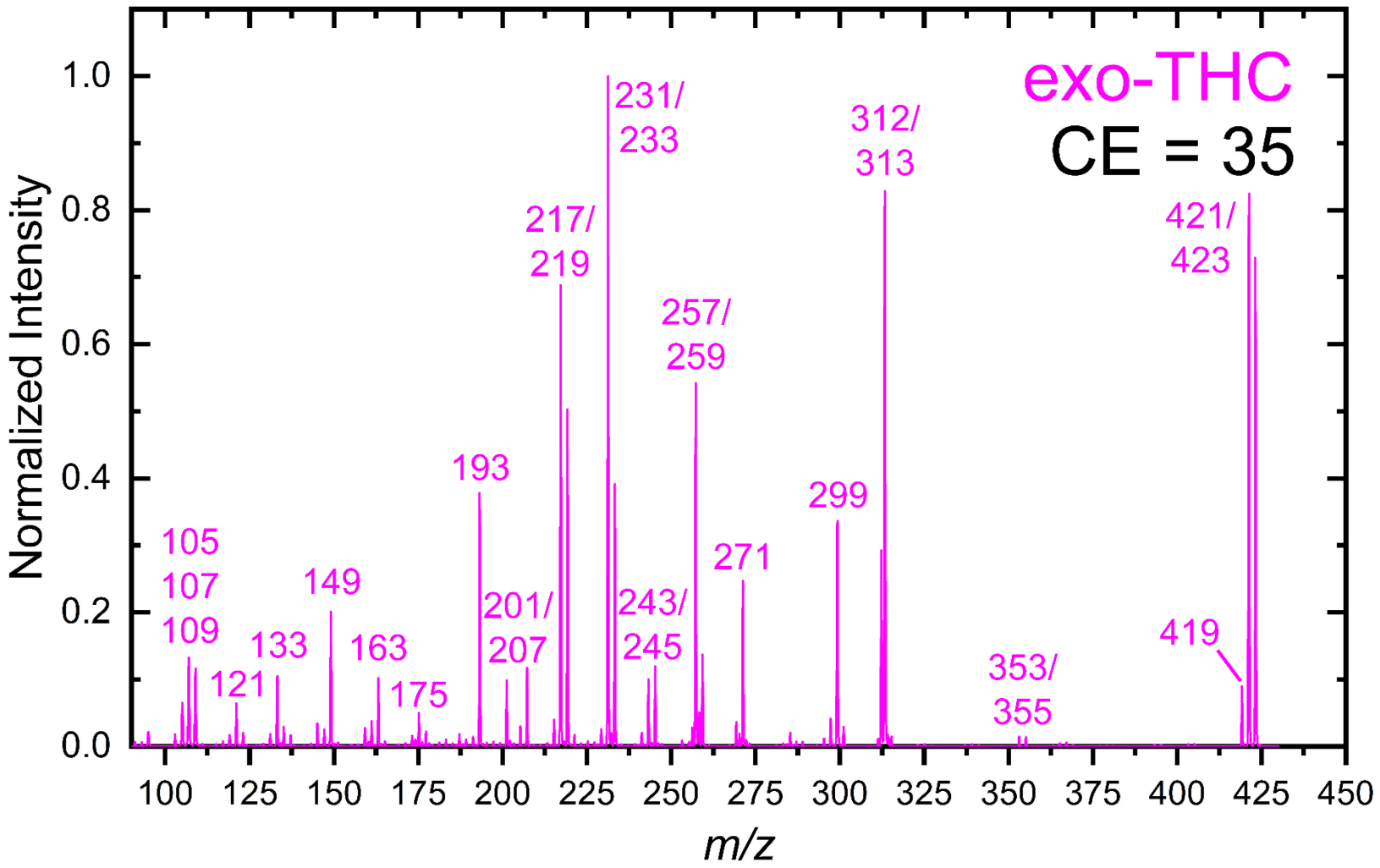

Figure S5-16. Product-ion spectrum of [exo-THC + Ag]$^+$ at CE = 35. Note that Q1 was modified to transmit both *m/z* 421 and 423 isotopologues of [exo-THC + Ag]$^+$.

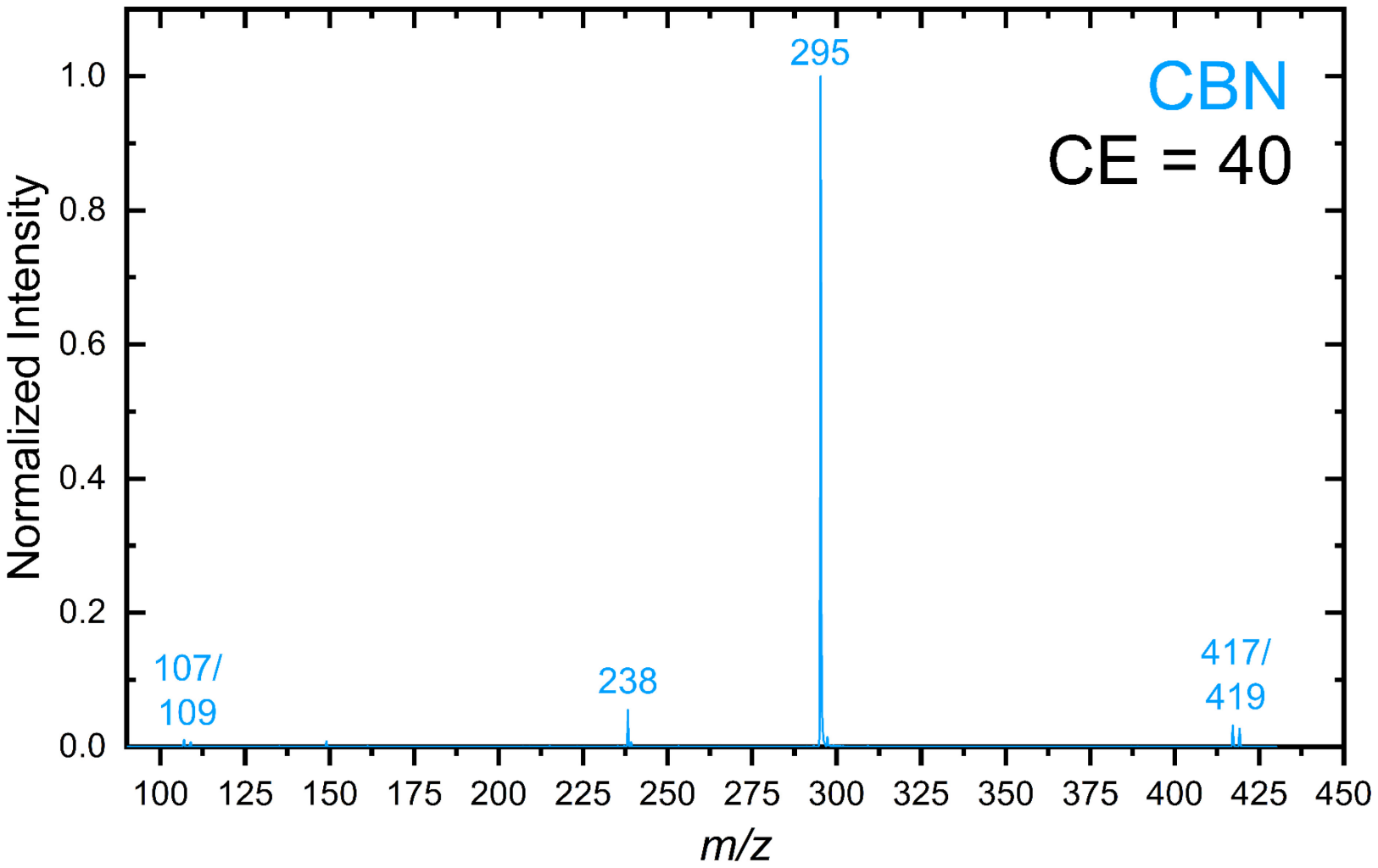

Figure S5-17. Product-ion spectrum of $[CBN + Ag]^+$ at CE = 40. Note that Q1 was modified to transmit both *m/z* 417 and 419 isotopologues of $[CBN + Ag]^+$.

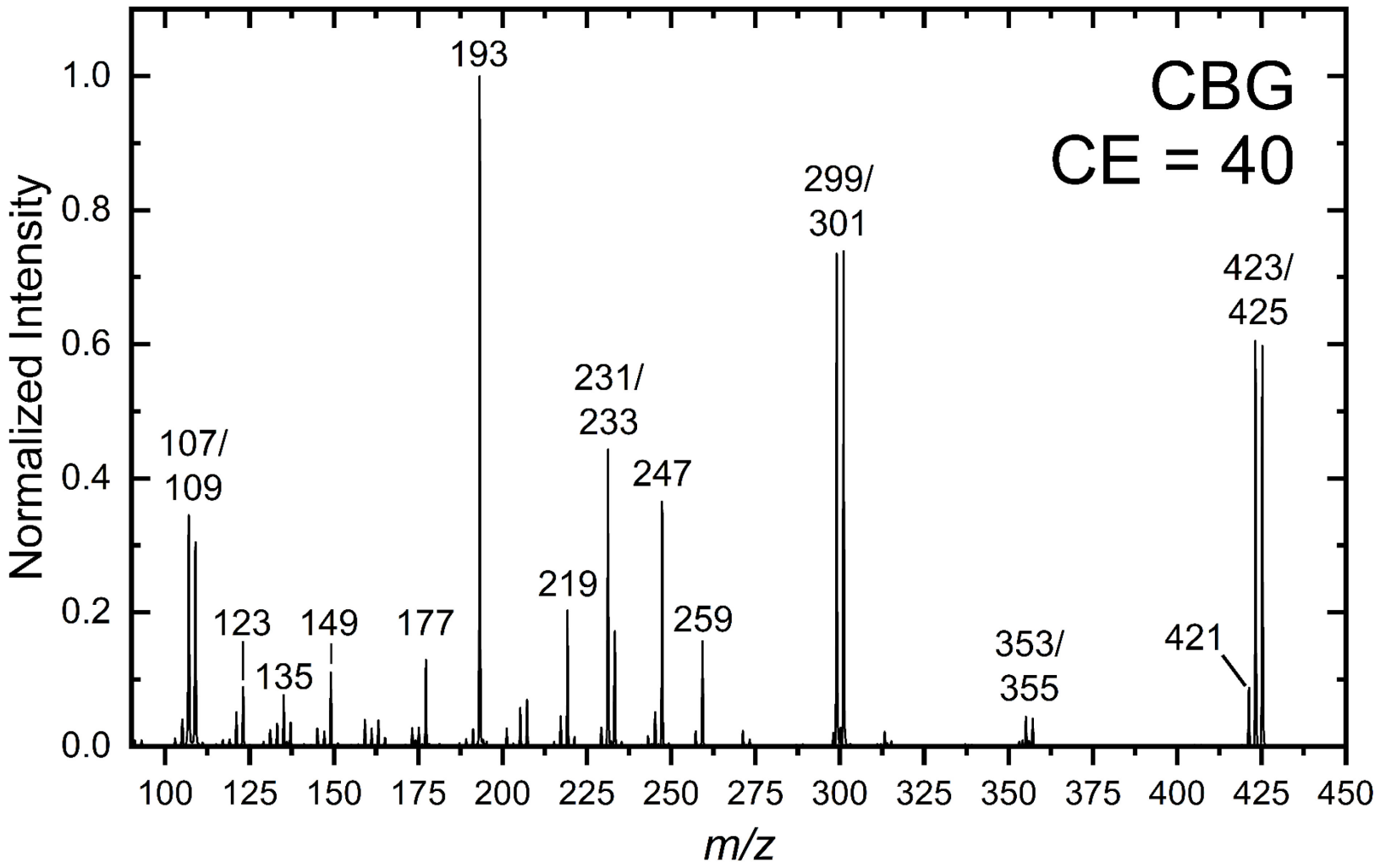

Figure S5-18. Product-ion spectrum of $[CBG + Ag]^+$ at CE = 40. Note that Q1 was modified to transmit both *m/z* 423 and 425 isotopologues of $[CBG + Ag]^+$.

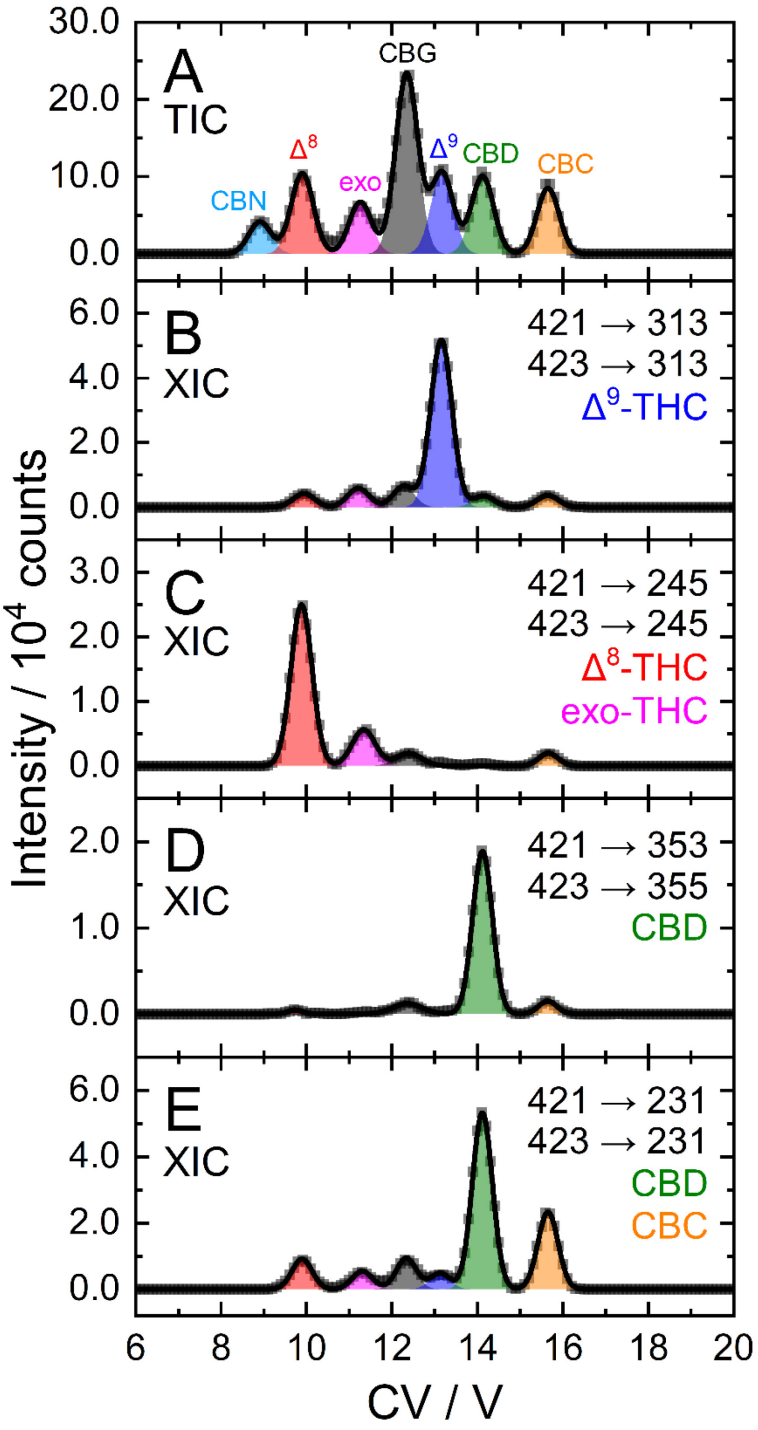

Figure S5-19. (**A**) Total ion chromatogram (TIC) and (**B** – **E**) extracted ion chromatograms (XIC) from a specific MRM transition for the separation of argentinated Δ^8-THC (red), Δ^9-THC (blue), CBC (orange), CBD (green), exo-THC (magenta), CBN (cyan), and CBG (black) by DMS-MS. Ionograms were obtained in a pure N_2 environment at SV = 4500 V, DP = 0 V, and DT = 50 °C from a mixture containing Δ^8-THC (500 ppb), Δ^9-THC (500 ppb), CBD (100 ppb), CBC (100 ppb), exo-THC (500 ppb), CBN (500 ppb), CBG (100 ppb), and AgOAc (10 ppm) in MeOH.

Figure S5-20. Packaging of the Full Spectrum Hemp Multicannabinoid Oil extract produced by NuLeaf Naturals. At the top, the concentration of CBN, Δ^9-THC, CBG, CBD, and CBC is stated to be 12 mg mL^{-1}, yet below, the amount of cannabinoid per activation (1 activation = 0.5 mL) leads to concentrations of 12.0 mg mL^{-1} for CBN, CBG, CBD, and CBC, but 13.6 for Δ^9-THC. This is also reflected in the mg g^{-1} equivalent, which we assume is determined from the density of the oil.

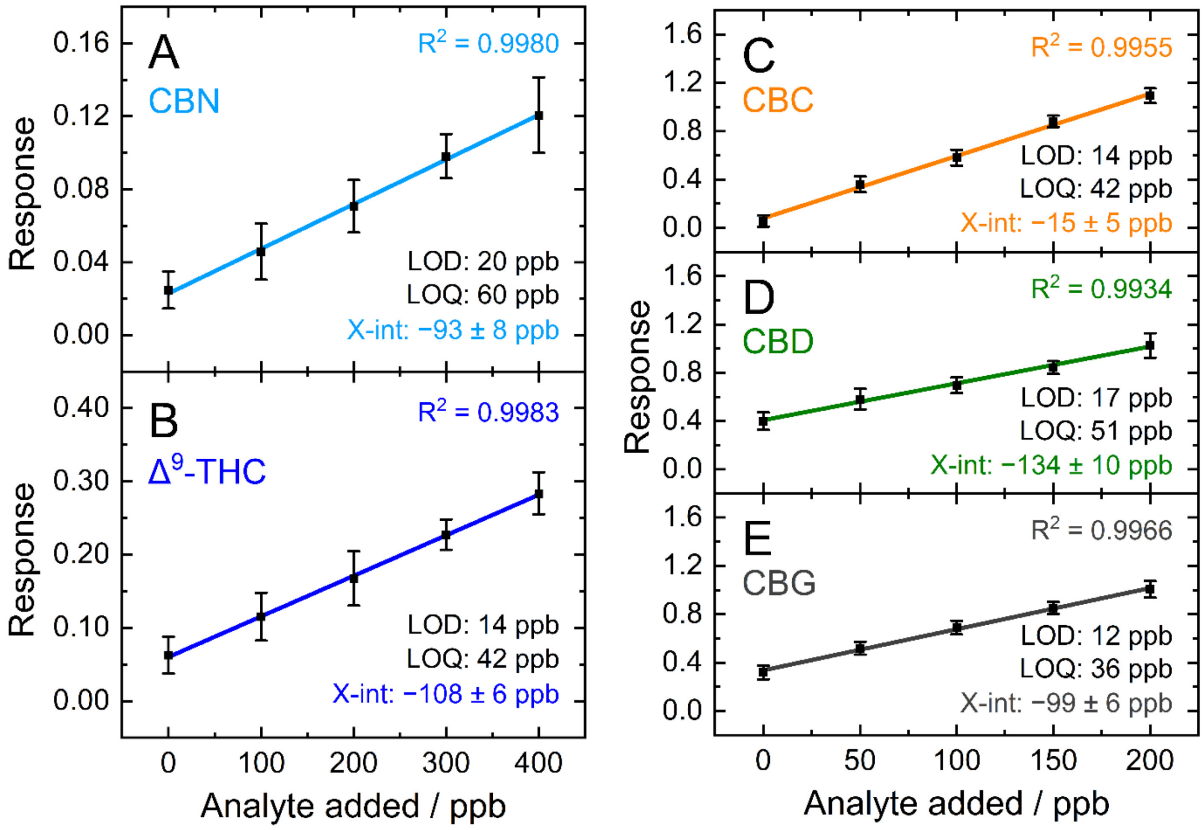

Figure S5-21. Calibration curves from concurrent standard additions of (**A**) CBN, (**B**) Δ^9-THC, (**C**) CBC, and (**D**) CBD, and (**E**) CBG to the NuLeaf extract (133333.3-fold dilution in MeOH and doped with 10 ppm of AgOAc). Error bars correspond to the standard deviation of the analyte response relative to the internal standard (CBDA; 300 ppb) across three replicate measurements. Limits of detection (LOD) and limits of quantitation (LOQ) are using Equations 4 and 5 (see main text).

Table S5-1. MRM transitions of the deprotonated forms of Δ^8-THC, Δ^9-THC, CBD, and CBC [*i.e.,* M – H]$^-$, along with the cannabinoids that appear within the extracted ion chromatogram (XIC) upon separation by DMS-MS.

Q1	Q3	CE / V	Cannabinoids present in XIC
313	313	17	Δ^8-THC, Δ^9-THC, CBD, CBC
313	245	10	Δ^8-THC, Δ^9-THC, CBD
313	191	24	Δ^8-THC, Δ^9-THC, CBD, CBC
313	179	24	Δ^8-THC, Δ^9-THC, CBD, CBC

Table S5-2. MRM transitions of the argentinated cannabinoids [M + Ag]$^+$. Cannabinoids in bold are the major peak in the extracted ion chromatogram (XIC), whereas cannabinoids in brackets are present in small quantities in the XIC (< 4 %).

Q1	Q3	CE / V	Cannabinoids present in XIC
421/423	313	17	**Δ^9-THC** (Δ^8-THC, exo-THC, CBD, CBC)
421/423	245	10	**Δ^8-THC** (exo-THC, CBG, Δ^9-THC, CBD, CBC)
421/423	353	24	**CBD** (Δ^8-THC, exo-THC, CBG, Δ^9-THC, CBD, CBC)
421/423	355	24	**CBD** (Δ^8-THC, exo-THC, CBG, Δ^9-THC, CBD, CBC)
421/423	231		**CBD, CBC** (Δ^8-THC, exo-THC, CBG, Δ^9-THC)
421/423	219		**Exo-THC** (Δ^8-THC, Δ^9-THC, CBC)
417/419	295		**CBN**
423/425	301		**CBG** (Δ^8-THC, exo-THC, Δ^9-THC, CBD, CBC)
423/425	193		**CBG** (Δ^8-THC, exo-THC, Δ^9-THC, CBD, CBC)

Table S5-3. Operating conditions of the ESI-DMS-QTRAP5500.

Parameter	Setting
Source	
Curtain Gas (CUR)	20.0
Collision gas (CAD)	High (12.0)
Ion spray voltage (IS)	5500
Source Temperature (TEM)	50
Nebulizing Gas Pressure (GS1)	30.0
Auxiliary Gas Pressure (GS2)	20.0
Compound	
Declustering Potential (DP)	100
Entrance Potential (EP)	10
Collision Energy (CE)	Varies
Collision Cell Exit Potential (CXP)	15
DMS	
DMS Temperature (DT)	50, 150, 225, 300
Modifier (MD)	Pure N_2 or N_2 with 1.5 mol% IPA
Separation Voltage (SV)	4400 V
Compensation Voltage (CV)	Varies
DMS Offset (DMO)	−3.0
DMS Resolution Enhancement (DR)	Varies (0 – 35 psi)
Resolution – Quad 1	
Ion Energy 1 (IE1)	1.1
Q1 Resolution	Unit
Resolution – Quad 3	
Ion Energy 3 (IE3)	1.8
Q3 Resolution	Unit
Detector	
CEM (CEM)	2100.0

Supplementary Sections

Section 5-1. Computational Methods

Quantum-chemical calculations were performed to assess the affinity of each cannabinoid for argentination. Briefly, candidate geometries for the neutral and argentinated form of Δ^8-THC, Δ^9-THC, CBD, CBC, cannabinol (CBN), cannabigerol (CBG), and exo-THC were generated manually. Each candidate structure was used as an input for the Conformer-Rotamer Ensemble Sampling Tool (CREST),[1,2] which generated a series of low-energy structures using the GFN2-xTB semiempirical tight-binding model.[3] For each neutral and argentinated cannabinoid, all structures generated by CREST that were within 25 kJ mol^{-1} of the lowest energy conformer were extracted and additionally sorted by cosine similarity,[4] yielding 5 – 30 representative conformers. Each of the unique conformers was carried forward for optimization at the ωB97X-D3/Def2-TZVPP level of theory, which employed the RIJcosX approximation and the Def2/J auxiliary basis set.[5–9] Normal mode analyses were conducted to ensure that each structure corresponded to a true minimum (*i.e.,* no imaginary frequencies) and to calculate thermochemical corrections. Electronic energies of the optimized structures were refined with single-point energy calculations conducted at the DLPNO-CCSD(T)/Def2-TZVPP level of theory, which used the Def2/C auxiliary basis set.[10–13] Thermochemical quantities were determined by combining DLPNO-CCSD(T) single point electronic energies with ωB97X-D3 thermochemistry, which we report as DLPNO-CCSD(T)/Def2-TZVPP//ωB97X-D3/Def2-TZVPP. All *ab initio* and density functional theory (DFT) calculations were performed using the ORCA computational package (version 5.0.3).[14–17] Results of the quantum-chemical calculations are provided in the ioChem-BD database entry associated with this manuscript (https://doi.org/10.19061/iochem-bd-6-225).[18] For the convenience of the reader, the structures of the lowest energy configuration of each argentinated and neutral cannabinoid are provided in Figure S5-22.

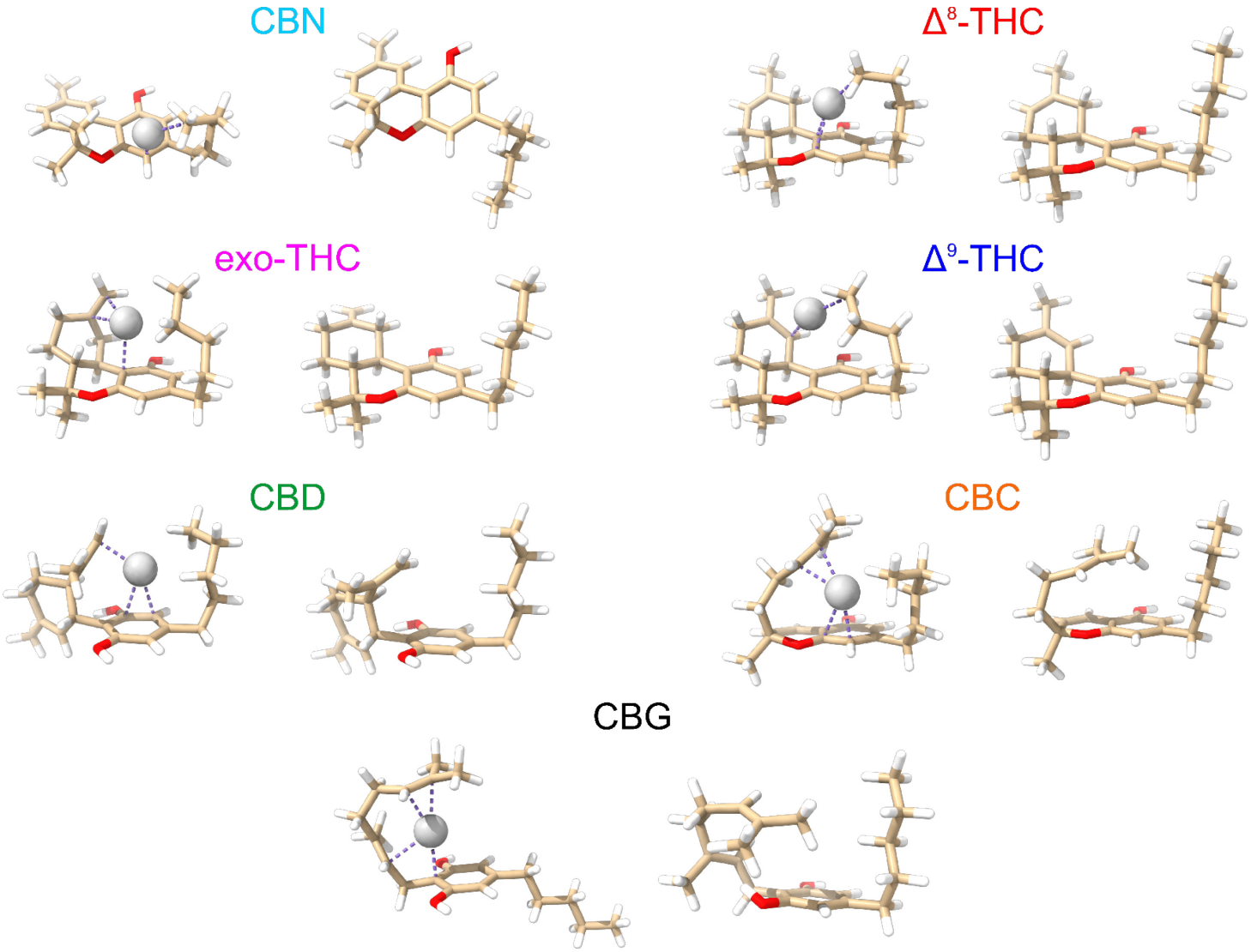

Figure S5-22. Lowest energy structure of the argentinated forms (*i.e.,* $[M + Ag]^+$) and neutral forms of CBN, Δ^8-THC, exo-THC, Δ^9-THC, CBD, CBC, and CBG, as determined at the DLPNO-CCSD(T)/Def2-TZVPP//ωB97X-D3/Def2-TZVPP level of theory.

The affinity of each cannabinoid for argentination is determined by the Gibbs energy of association (ΔG_{ass}; Equation S5-1) , where G_{Ag^+}, G_M, and $G_{[M+Ag]^+}$ are the Gibbs energies of the silver cation, neutral cannabinoid, and argentinated cannabinoid, respectively. Calculation of ΔG_{ass} uses weighted Gibbs energies, where the population ρ of the n^{th} isomer in an ensemble is determined by its Gibbs corrected electronic energy, G_n, (Equation S5-2; T = 298 K). The Gibbs energy of the ensemble, G, is given by the product of the n^{th} isomer's population and Gibbs energy, summed over all n isomers (Equation S5-3).

$$\Delta G_{ass} = (G_{Ag^+}) + (G_M) - (G_{[M+Ag]^+}) \qquad \textit{Eq S5-1}$$

$$\rho_n = \frac{\exp\left(\frac{G_n}{(RT)}\right)}{\sum_n \exp\left(\frac{G_n}{(RT)}\right)} \qquad \textit{Eq S5-2}$$

$$G = \sum_n \rho_n G_n \qquad \textit{Eq S5-3}$$

Section S5-2. Computational investigation of the fragmentation behaviour of argentinated Δ^8-THC, Δ^9-THC, CBD, and CBC.

The distinct fragmentation patterns of the argentinated cannabinoid isomers is an intriguing observation, and one which is worthy of thorough investigation. Such an investigation would entail a detailed mapping of the reaction profile of each fragmentation path inclusive of transition states, as the kinetics of fragmentation during CID is especially important is rationalizing MS^2 behaviour. However, such a study is worthy of publication in its own right. Until such studies can be completed, we can gain insight into the MS^2 behaviour of each argentinated cannabinoid isobar by looking at the Gibbs energy associated with the proposed fragmentation pathways outlined in Figure S5-23 (ΔG_{CID}; Equation S5-4). Here, G_{Frag^+} is the Gibbs energy of the cationic fragment, G_{Frag} is the Gibbs energy of the neutral fragment, and $G_{[M+Ag]^+}$ is the Gibbs energy of the intact, argentinated cannabinoid (*e.g.,* [Δ^9-THC + Ag]$^+$).

$$\Delta G_{CID} = (G_{Frag^+}) + (G_{Frag}) - (G_{[M+Ag]^+}) \qquad Eq\ S4$$

Analysis of the ΔG_{CID} values indicates that fragmentation pathways exhibit values that are in line with other computed values from previous computational studies.[19] Table S5-4 compares the ΔG_{CID} for each possible product ion that originates from a particular argentinated precursor. For example, both [Δ^9-THC + Ag]$^+$ and [Δ^8-THC + Ag]$^+$ produce a fragment ion with a *m/z* of 313, except this fragment is only formed in small quantities from [Δ^8-THC + Ag]$^+$ but is the major fragment product from [Δ^9-THC + Ag]$^+$. This is reflected in the lower ΔG_{CID} value for the [Δ^9-THC + Ag]$^+$ fragmentation pathway relative to the fragmentation of [Δ^8-THC + Ag]$^+$.

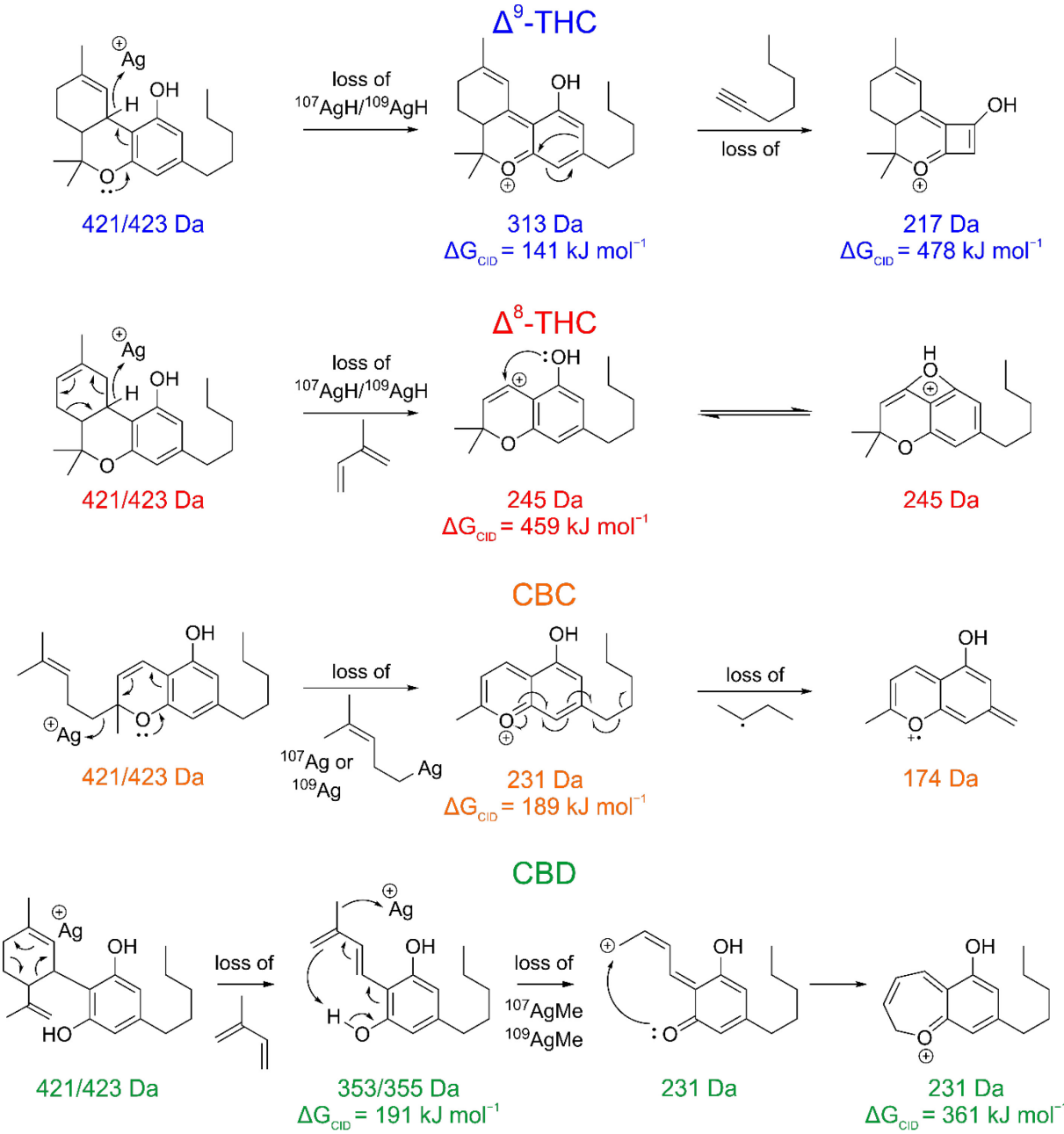

Figure S23. Proposed mechanisms of formation for the major product ions observed in the MS^2 spectra of $[\Delta^9\text{-THC} + Ag]^+$ (blue), $[\Delta^8\text{-THC} + Ag]^+$ (red), $[CBC + Ag]^+$ (orange), and $[CBD + Ag]^+$ (green). ΔG_{CID} values are reported at the DLPNO-CCSD(T)/Def2-TZVPP//ωB97X-D3/Def2-TZVPP level of theory.

Table S4. Comparison of ΔG_{CID} values (in kJ mol^{-1}) for the fragments shown in Figure S5-23, as calculated at the DLPNO-CCSD(T)/Def2-TZVPP//ωB97X-D3/Def2-TZVPP level of theory.

Cannabinoid	*m/z* 353/355	*m/z* 313	*m/z* 245	*m/z* 231
[Δ^9-THC + Ag]$^+$	–	141.3	–	–
[Δ^8-THC + Ag]$^+$	–	165.2	459.5	–
[CBC + Ag]$^+$	–	–	–	188.9
[CBD + Ag]$^+$	191.0	–	–	361.5

Section S5-3. Computational investigation of the fragmentation behaviour of argentinated exo-THC, CBN, and CBG.

Analogously to the results presented in Supplementary Section S2, ΔG_{CID} values were computed for the major fragments originating from CID of the argentinated forms of exo-THC, CBN, and CBG. The proposed mechanisms of the formation of each fragment ion, alongside its respective ΔG_{CID}, are provided below.

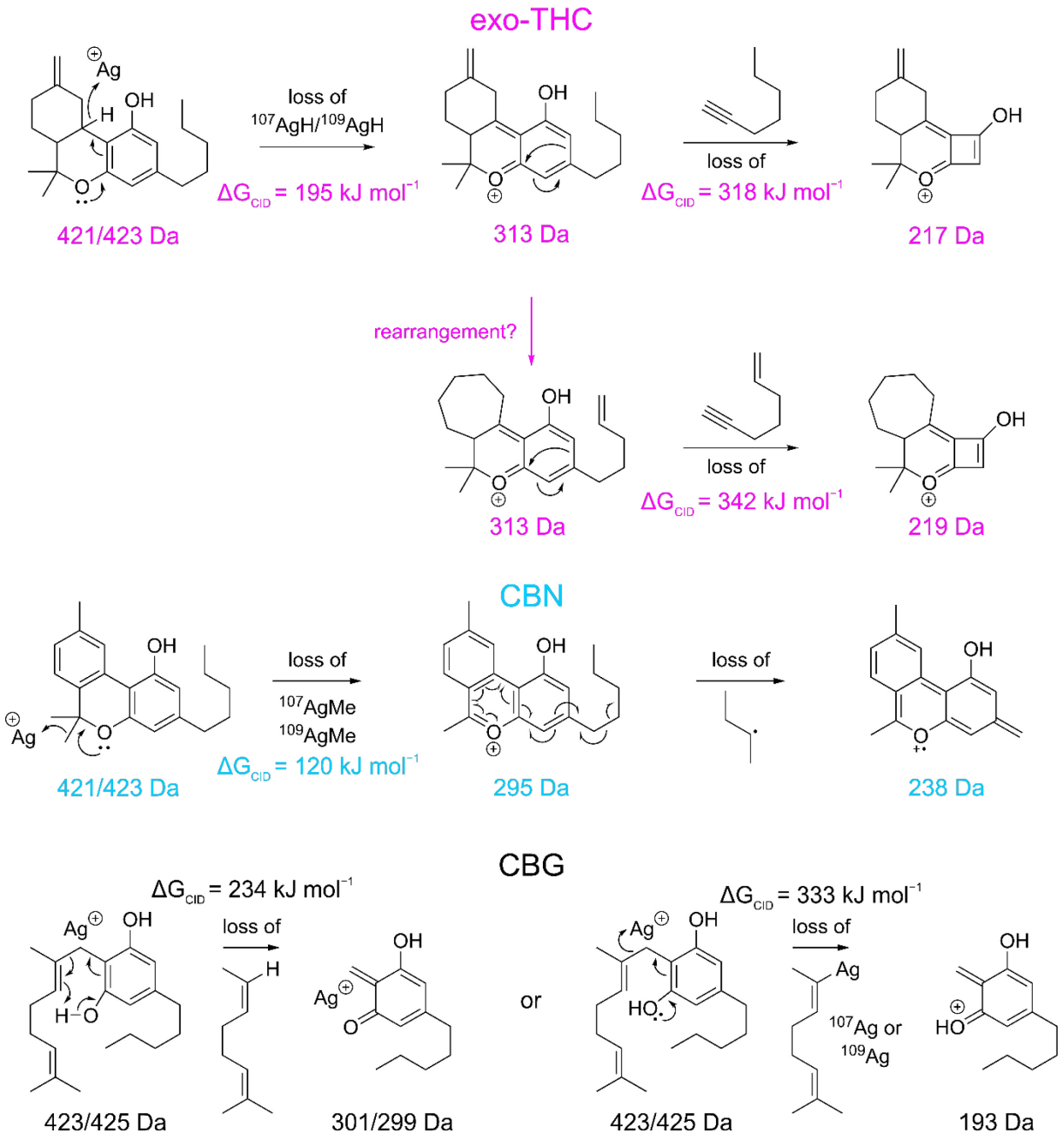

Section 5-4. Frequently Asked Questions

1. **Are there any potential ramifications to instrument performance associated with infusing ~ 5ppm for AgOAc for prolonged periods of time?**

Some caution should always be taken when working with salt adducts, especially silver salts. Our experience has found that AgOAc is preferable to $AgNO_3$ in terms of preventing Ag buildup within the source and DMS cell. In the context of this work, the concentration of AgOAc is kept reasonably low (5 ppm or less) and does not cause and prolonged contamination within our system. A simple wipe of the curtain plate with a KimWipe lightly dipped in 1:1 MeOH/H2O removes the small amounts of silver that get deposited, and a flow of 1:1 MeOH/H2O for ~ 10 minutes removes all traces of silver and the argentinated cannabinoids from the DMS-MS system.

References

(1) Grimme, S. Exploration of Chemical Compound, Conformer, and Reaction Space with Meta-Dynamics Simulations Based on Tight-Binding Quantum Chemical Calculations. *J Chem Theory Comput* **2019**, *15* (5), 2847–2862. https://doi.org/10.1021/acs.jctc.9b00143.

(2) Pracht, P.; Bohle, F.; Grimme, S. Automated Exploration of the Low-Energy Chemical Space with Fast Quantum Chemical Methods. *Physical Chemistry Chemical Physics* **2020**, *22* (14), 7169–7192. https://doi.org/10.1039/C9CP06869D.

(3) Bannwarth, C.; Ehlert, S.; Grimme, S. GFN2-XTB - An Accurate and Broadly Parametrized Self-Consistent Tight-Binding Quantum Chemical Method with Multipole Electrostatics and Density-Dependent Dispersion Contributions. *J Chem Theory Comput* **2019**, *15* (3), 1652–1671. https://doi.org/10.1021/acs.jctc.8b01176.

(4) Zhou, C.; Ieritano, C.; Hopkins, W. S. Augmenting Basin-Hopping With Techniques From Unsupervised Machine Learning: Applications in Spectroscopy and Ion Mobility. *Front Chem* **2019**, *7*, 519. https://doi.org/10.3389/fchem.2019.00519.

(5) Grimme, S.; Antony, J.; Ehrlich, S.; Krieg, H. A Consistent and Accurate Ab Initio Parametrization of Density Functional Dispersion Correction (DFT-D) for the 94 Elements H-Pu. *Journal of Chemical Physics* **2010**, *132* (15), 154104. https://doi.org/10.1063/1.3382344.

(6) Ekström, U.; Visscher, L.; Bast, R.; Thorvaldsen, A. J.; Ruud, K. Arbitrary-Order Density Functional Response Theory from Automatic Differentiation. *J Chem Theory Comput* **2010**, *6* (7), 1971–1980. https://doi.org/10.1021/ct100117s.

(7) Andrae, D.; Häußermann, U.; Dolg, M.; Stoll, H.; Preuß, H. Energy-Adjusted Ab Initio Pseudopotentials for the Second and Third Row Transition Elements. *Theor Chim Acta* **1990**, *77* (2), 123–141. https://doi.org/10.1007/BF01114537.

(8) Weigend, F. Accurate Coulomb-Fitting Basis Sets for H to Rn. *Physical Chemistry Chemical Physics* **2006**, *8* (9), 1057–1065. https://doi.org/10.1039/b515623h.

(9) Weigend, F.; Ahlrichs, R. Balanced Basis Sets of Split Valence, Triple Zeta Valence and Quadruple Zeta Valence Quality for H to Rn: Design and Assessment of Accuracy. *Physical Chemistry Chemical Physics* **2005**, *7* (18), 3297–3305. https://doi.org/10.1039/b508541a.

(10) Riplinger, C.; Sandhoefer, B.; Hansen, A.; Neese, F. Natural Triple Excitations in Local Coupled Cluster Calculations with Pair Natural Orbitals. *Journal of Chemical Physics* **2013**, *139* (13), 134101. https://doi.org/10.1063/1.4821834.

(11) Riplinger, C.; Neese, F. An Efficient and near Linear Scaling Pair Natural Orbital Based Local Coupled Cluster Method. *Journal of Chemical Physics* **2013**, *138* (3), 34106. https://doi.org/10.1063/1.4773581.

(12) Riplinger, C.; Pinski, P.; Becker, U.; Valeev, E. F.; Neese, F. Sparse Maps - A Systematic Infrastructure for Reduced-Scaling Electronic Structure Methods. II. Linear Scaling Domain Based Pair Natural Orbital Coupled Cluster Theory. *Journal of Chemical Physics* **2016**, *144* (2), 24109. https://doi.org/10.1063/1.4939030.

(13) Hellweg, A.; Hättig, C.; Höfener, S.; Klopper, W. Optimized Accurate Auxiliary Basis Sets for RI-MP2 and RI-CC2 Calculations for the Atoms Rb to Rn. *Theor Chem Acc* **2007**, *117* (4), 587–597. https://doi.org/10.1007/s00214-007-0250-5.

(14) Neese, F. The ORCA Program System. *WIREs Computational Molecular Science* **2012**, *2* (1), 73–78. https://doi.org/10.1002/wcms.81.

(15) Valeev, E. F. *Libint: A library for the evaluation of molecular integrals of many-body operators over Gaussian functions, Version 2.6.0*. http://libint.valeyev.net/.

(16) Lehtola, S.; Steigemann, C.; Oliveira, M. J. T.; Marques, M. A. L. Recent Developments in LIBXC — A Comprehensive Library of Functionals for Density Functional Theory. *SoftwareX* **2018**, *7*, 1–5. https://doi.org/10.1016/j.softx.2017.11.002.

(17) Neese, F. Software Update: The ORCA Program System—Version 5.0. *WIREs Computational Molecular Science* **2022**, *12* (5), e1606. https://doi.org/10.1002/WCMS.1606.

(18) Álvarez-Moreno, M.; De Graaf, C.; López, N.; Maseras, F.; Poblet, J. M.; Bo, C. Managing the Computational Chemistry Big Data Problem: The IoChem-BD Platform. *J Chem Inf Model* **2015**, *55* (1), 95–103. https://doi.org/10.1021/ci500593j.

(19) Ieritano, C.; Hopkins, W. S. "Thermometer" Ions Can Fragment Through an Unexpected Intramolecular Elimination: These Are Not the Fragments You Are Looking For. *J Phys Chem Lett* **2021**, 5994–5999. https://doi.org/10.1021/acs.jpclett.1c01538.